Polishing of a 6.5 m f/1.25 mirror for the first Magellan telescope

H. M. Martin, R. G. Allen, J. H. Burge, L. R. Dettmann, D. A. Ketelsen, W. C. Kittrell and S. M. Miller

Steward Observatory, University of Arizona, Tucson, AZ 85721

ABSTRACT

We describe the optical fabrication and testing of the 6.5 m f/1.25 primary mirror for the first Magellan telescope. Figuring was performed with a 1.2 m stressed lap, which bends under active control to match the local curvature of the optical surface, and a variety of small passive tools. The figure was measured with IR and visible interferometers, using refractive null correctors to compensate 810 microns of aspheric departure. After subtraction of Seidel astigmatism and spherical aberration, the finished mirror is accurate to 14 nm rms surface error, and has an encircled energy of 80% in 0.06″ diameter at 500 nm.

Keywords: telescopes, optical fabrication, optical testing, aspheres

1. INTRODUCTION

The 6.5 m mirrors for the Multiple Mirror Telescope (MMT) Conversion and the first Magellan telescope are the first large mirrors cast and polished by the Steward Observatory Mirror Lab. Two Magellan telescopes are under construction at Las Campanas in Chile.[1] The primary mirrors for these and the MMT are identical honeycomb sandwiches, lightweighted by a factor of five to give a marked improvement in stiffness and thermal response. At f/1.25 they are much faster than other large mirrors. The short focal length allows a small, economical enclosure, a short, stiff telescope structure, and a wide field of view at the Cassegrain focus without an excessively large secondary.

Such fast mirrors present the challenge of polishing the extremely aspheric surface, and the Mirror Lab's polishing system is designed for that purpose. Most lapping operations are performed with a stressed lap that is relatively large (1.2 m) and stiff, and maintains fit through continuous active shape changes.[2-3] The Magellan mirror has a stringent accuracy requirement, corresponding to a seeing-limited image size of 0.086″ FWHM and a scattering loss due to small-scale structure of 1.5% (both at 500 nm wavelength).

2. FABRICATION

The fabrication process is similar to that described previously for the MMT mirror.[4-6] We form the mirror blank by spin-casting Ohara E6 borosilicate glass in a ceramic fiber mold. The mold contains 1020 hexagonal boxes that form the voids of the honeycomb. Molten glass flows between the boxes to form ribs 12 mm thick, and underneath the boxes (which are raised off the floor of the mold on spacers) to form a back plate 25 mm thick. The tops of the boxes are cut to form a parabolic surface, and the spin-casting creates a uniform layer that will be generated to a thickness of 28 mm.

Generating, loose-abrasive grinding and polishing are performed with the same machine, the 8.4 m capacity Large Optical Generator.[7] The LOG has the geometry of a vertical mill with all axes (including lap spindle) under computer control. We generate the front surface as a paraboloid to an accuracy of 5-10 microns rms. We also generate, lap and polish the flat rear surface, and edges and bevels around the front and rear surfaces.

For loose-abrasive grinding and polishing we use the same stressed lap, comprising a 1.5 m aluminum plate 50 mm thick and 18 moment-generating actuators around the edge of the plate to bend it elastically. Three more actuators apply lifting forces to control polishing pressure and pressure gradients. The bending actuators are programmed to make the lap shape match

the ideal parabolic mirror surface at all times, while the lifting actuators can be used to vary the pressure according to the current figure error—applying more pressure at the high points—and to balance forces when the lap extends over the edge of the mirror. The polishing surface is usually restricted to a maximum diameter of 1.2 m, because of small-scale shape errors at the edge due to the discrete bending actuators.

The polishing machine provides dynamic control of the speeds of its three polishing motions (radial, mirror rotation and lap rotation). We generally use the radial motion and lap rotation to control axisymmetric figure errors. Variations in pressure and mirror rotation rate can be used to remove non-axisymmetric errors. We control mechanical quilting of the honeycomb structure under polishing pressure by applying an equal air pressure to the inside of the mirror. We use stiff passive tools of 10-40 cm diameter for local figuring on scales of 20-60 cm.

All lapping operations are guided by phase-shifting interferometry. We use a 10.6 micron interferometer for loose-abrasive grinding and early polishing, and a visible wavelength interferometer for the final figuring. Separate IR and visible null lenses correct the 810 micron departure from the best-fitting sphere. We measured the accuracy of both null lenses using small computer-generated holograms that mimic the ideal primary mirror.[8] Measurement of the visible hologram with the visible null lens revealed significant discrepancies on two occasions. In both cases we eventually traced the problem to an error in refractive index of the large relay element of the null lens.

We ventilate the internal surfaces of the honeycomb after each polishing run in order to enhance thermal equilibration. (A similar ventilation system is used in the telescope.) For polishing and testing, the mirror is supported on a passive hydraulic whiffletree, with forces matching the active support system to be used in the telescope.[9] We monitored support forces at the 104 support locations and found that some varied by up to 30 N, probably due to a combination of leakage and friction in the passive hydraulic supports. These force variations produce astigmatism at a level on the order of 400 nm peak-to-valley surface, and smaller amounts of other flexible bending modes. Variations on this order were observed from day to day. We decided to correct astigmatism with the active supports in the telescope rather than by polishing it out.

3. RESULTS

We present the final results in the form of a surface contour map, synthetic interference pattern, and diffraction calculations. All data are based on an average of 150 phase maps. The spatial resolution is 200 pixels across the mirror. The noise in an individual map, caused primarily by turbulence, averages about 50 nm rms surface error and shows little correlation between maps. The noise in the average should be less than 10 nm rms. Tilt, focus and coma, which result from slight misalignment of the interferometer with respect to the optical axis of the mirror, have been subtracted.

Seidel astigmatism and spherical aberration have also been subtracted. The final astigmatism of 540 nm peak-to-valley surface will be corrected in the telescope by maximum support forces of about 5 N. These correction forces will be determined empirically when the mirror is installed in its active support cell in the lab.[10] The final spherical aberration of 60 nm peak-to-valley surface is within the uncertainty of the null lens and will be corrected in the telescope by the spacing of the optics.

Figure 1 shows the surface contour map and synthetic interferogram. Figure 2 shows encircled energy diagrams in a perfect atmosphere and in 0.25″ seeing, roughly the best seeing expected. These are based on the full-aperture measurement of Figure 1. In perfect seeing the mirror focuses 80% of the light at 500 nm into a 0.06″ diameter.

A set of subaperture measurements was made as a check on small-scale structure that might not be resolved in the full-aperture maps. These maps, shown in Figure 3, have 2.2 times the resolution of the full-aperture maps. In subaperture maps one cannot completely distinguish alignment aberrations (those caused by slight misalignment of the interferometer) from large-scale figure errors. We have subtracted tilt, focus, astigmatism and coma, fit in local coordinates for each subaperture. While this correction removes more than alignment errors, all errors removed are already well measured in the full-aperture map, and are easily controlled with the active supports.

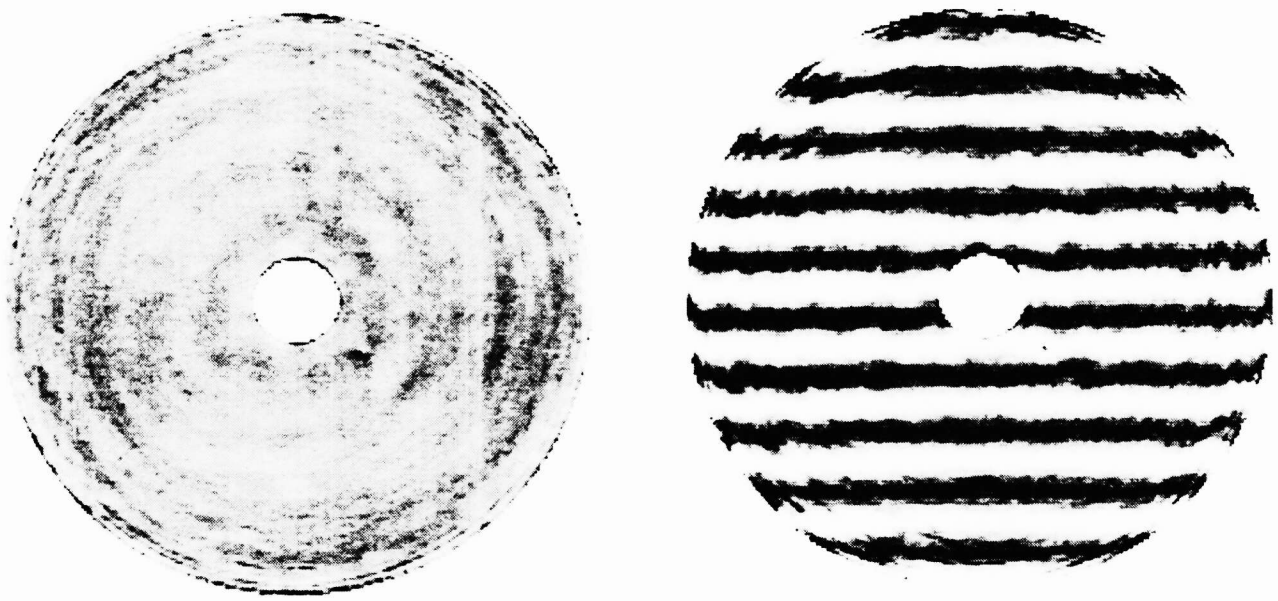

Figure 1. Gray-scale map of the mirror surface and synthetic interferogram for the Magellan mirror with astigmatism and spherical aberration subtracted. The gray scale covers ±100 nm of surface and the rms surface error is 14 nm. The interferogram is calculated for a wavelength of 633 nm. The displays cover the full polished surface.

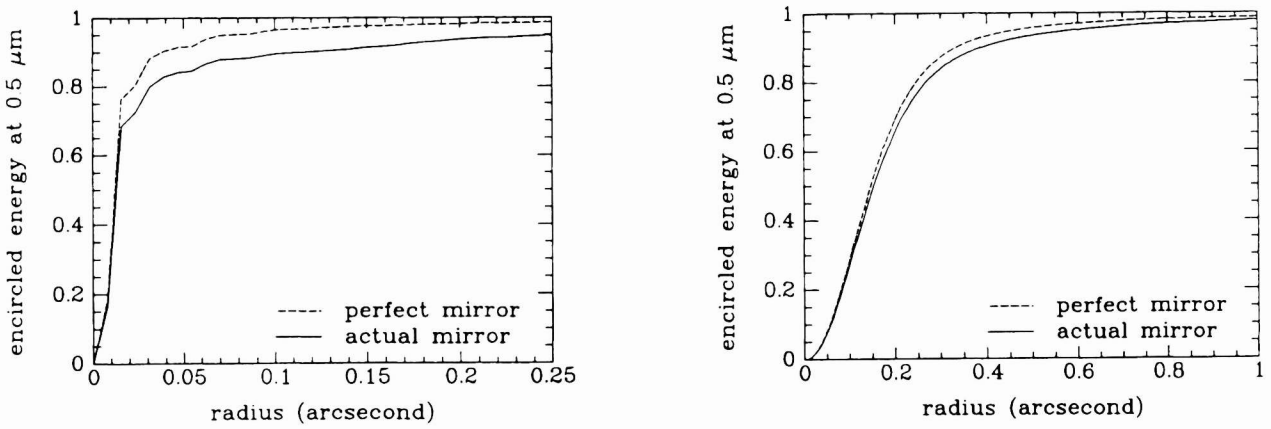

Figure 2. Encircled energy as a function of radius for the Magellan mirror and for a perfect mirror. Left: in perfect seeing. Right: in seeing of 0.25″ FWHM.

4. STRENGTHS AND LIMITATIONS OF STRESSED-LAP POLISHING

The Mirror Lab's polishing system has succeeded in achieving a very accurate surface on one of the most challenging large telescope mirrors ever made. The process was efficient, with all lapping operations completed in eight calendar months. Still, with the prospect of additional 6.5 m mirrors and at least two 8.4 m mirrors to polish, and unknown future applications, we want to make further improvements in efficiency. This must start with an understanding of the limitations of the present system.

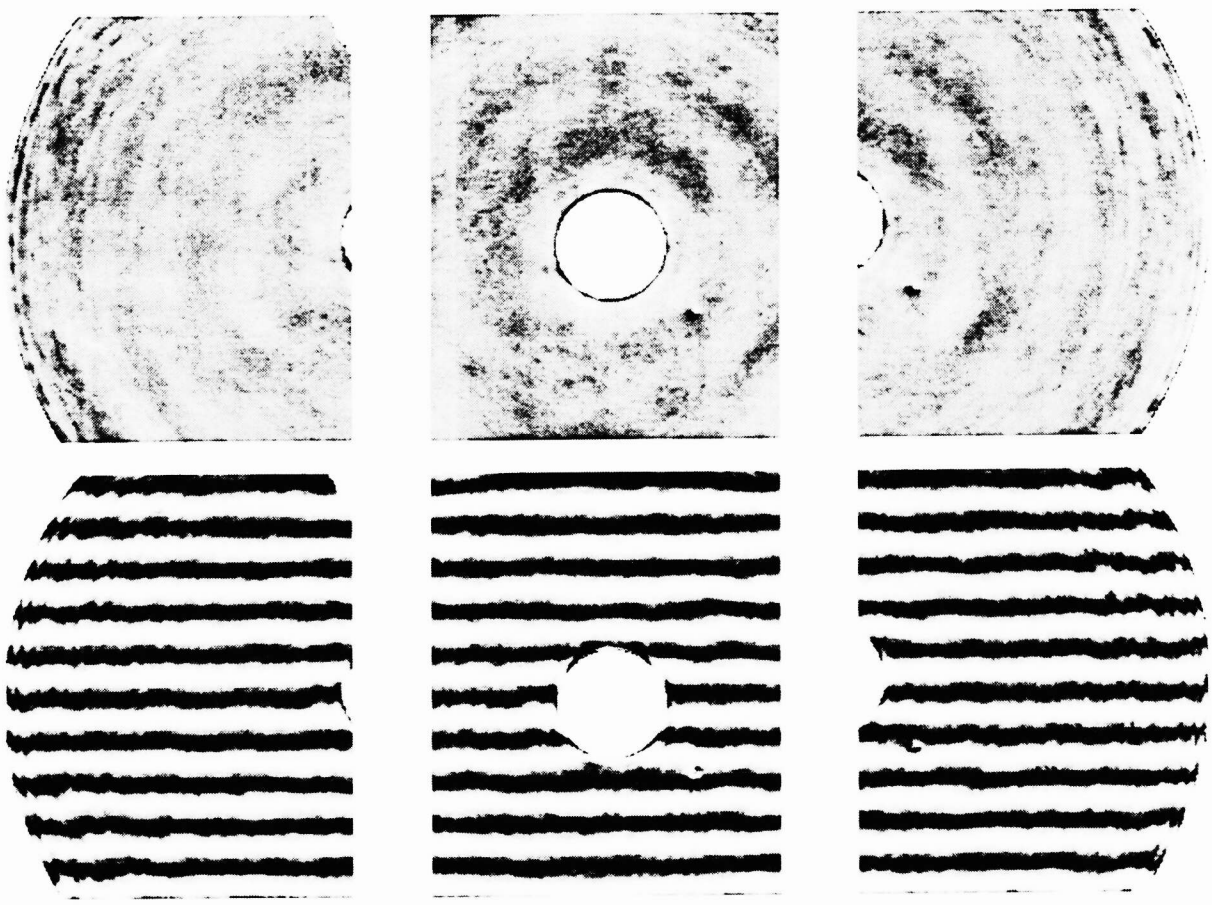

Figure 3. Gray-scale contour maps and synthetic interference patterns for three subapertures. The gray scale covers ±100 nm of surface. The interference patterns are calculated for a wavelength of 633 nm. The displays extend to the edges of the polished surface.

We developed stressed-lap polishing with the goal of making large, highly aspheric mirrors as if they were spheres. In spherical polishing, it is advantageous to use a large, stiff lap in order to maximize passive smoothing action. Our goal with the stressed lap is to maintain that strong passive smoothing for steep aspheres. The lap can be large and stiff because it bends actively to match the curvature variations of the mirror. Ideally, it would make the mirror's asphericity transparent to the optician.

In practice there are limits to this ideal model. These are related to the finite accuracy of the lap's shape changes, and the fact that we use only one stressed lap of fixed diameter. Considerations of weight and stiffness led to the choice of a 1.5 m diameter aluminum plate 50 mm thick. We use the central 1.2 m diameter as the polishing surface because the discrete bending actuators create local shape errors near the edge. This polishing surface can be reduced to about 0.8 m diameter by changing the distribution of pitch, but further reduction is difficult because the lap becomes unstable, in the sense that small errors in moment applied by the lifting actuators cause large pressure gradients. Furthermore, frequent changes in pitch area are inefficient because of the time required to apply new pitch and press it to shape.

In order to understand the strengths and limitations of this technique, it is useful to distinguish between figuring, which is the selective removal of glass at identified positions on the mirror, and smoothing, which is the natural tendency to reduce errors at high spatial frequency because the lap only contacts (or exerts greater pressure on) the high spots. Our 1.2 m lap is effective at figuring on scales on the order of 1 m and larger, and effective at smoothing over some range of scales below about 1 m. The efficiency of smoothing depends on the stiffness of the lap, the accuracy of its shape changes, and the amplitude and scale of the errors.

Our ability to control errors of mid spatial frequency, on the order of 1 m, depends on obtaining an overlap between the scales on which we can figure and those on which we can smooth. We want to push the figuring to smaller scales and the smoothing to larger scales. We have found that we do not have sufficient overlap to obtain the desired surface accuracy on all scales with the stressed lap alone. While do not fully understand the limitations of either process, we have a rough model of them that is illustrated by the accuracy achieved at various stages.

The convergence curve for loose-abrasive grinding and polishing is shown in Figure 4. The figure shows rms surface error after removal of Seidel astigmatism and spherical aberration. While the accuracy criterion for this mirror is a structure function, which includes information on all spatial scales, the corrected rms surface error represents the progress fairly well. A total of 79 iterations were run between March 17 and November 11, 1998. The average improvement in rms surface error was 17% per iteration during loose-abrasive grinding and 4.5% during polishing.

Figure 4. Convergence during loose-abrasive grinding and polishing, represented by rms surface error. Seidel astigmatism and spherical aberration have been subtracted. Some irregularities, such as the spike at iteration 77, are related to problems with support forces or lack of thermal equilibrium.

We used the stressed lap exclusively through iteration 52, with an rms surface error of 51 nm and figure shown in Figure 5. The error was dominated by several axisymmetric zones, the most difficult near the outer edge. At that point we started using passive laps to control the outer 40 cm of the mirror. Laps of 10-20 cm diameter were used, constrained in rotation and with short radial strokes in order to limit the misfit. This technique was very effective at removing the dominant high zone, but slight departures from the desired removal occasionally introduced narrow features. (One of these can be seen in Figure 6.) Continued passive smoothing with the stressed lap reduced these to an acceptable level. This combination was used through iteration 71, with an rms surface error of 22 nm and figure shown in Figure 6. Several zones with unacceptable slopes remained. For the final eight iterations we used passive laps on four interior zones in addition to the outer edge, and continued passive smoothing with the stressed lap. The final accuracy was 14 nm rms surface, shown in Figure 7.

It is interesting to compare the required figure accuracy with the amplitude of asphericity that must be maintained accurately. The dashed curve in Figure 7 illustrates that the aspheric departure is more than four orders of magnitude greater than the final accuracy. Apart from the lap bending, there is no natural tendency to maintain this aspheric figure. The 1.2 m lap bends to follow the desired 810 microns of aspheric departure while controlling undesired features at the 20 nm level.

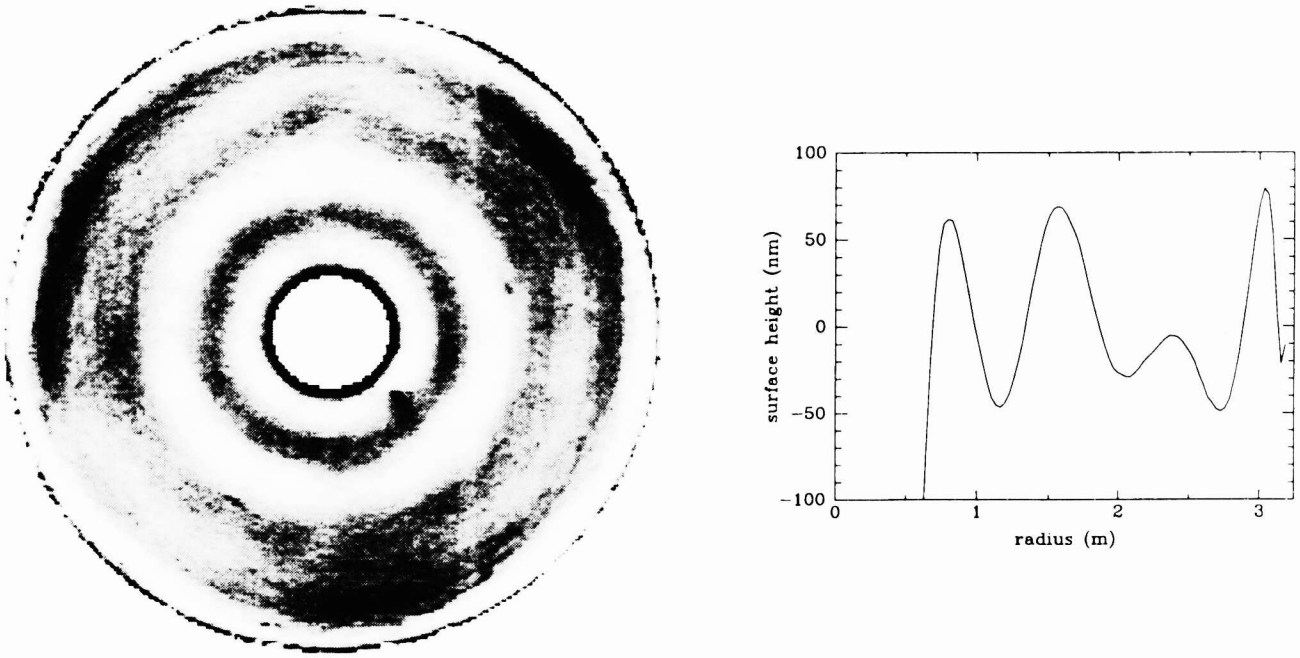

Figure 5. Gray-scale surface map and average radial profile at iteration 52, immediately before the first polishing run with a passive lap at the outer edge. The gray scale covers ±100 nm of surface, and the image covers a diameter of 6.38 m, the outer 6 cm lost due to a rolled edge.

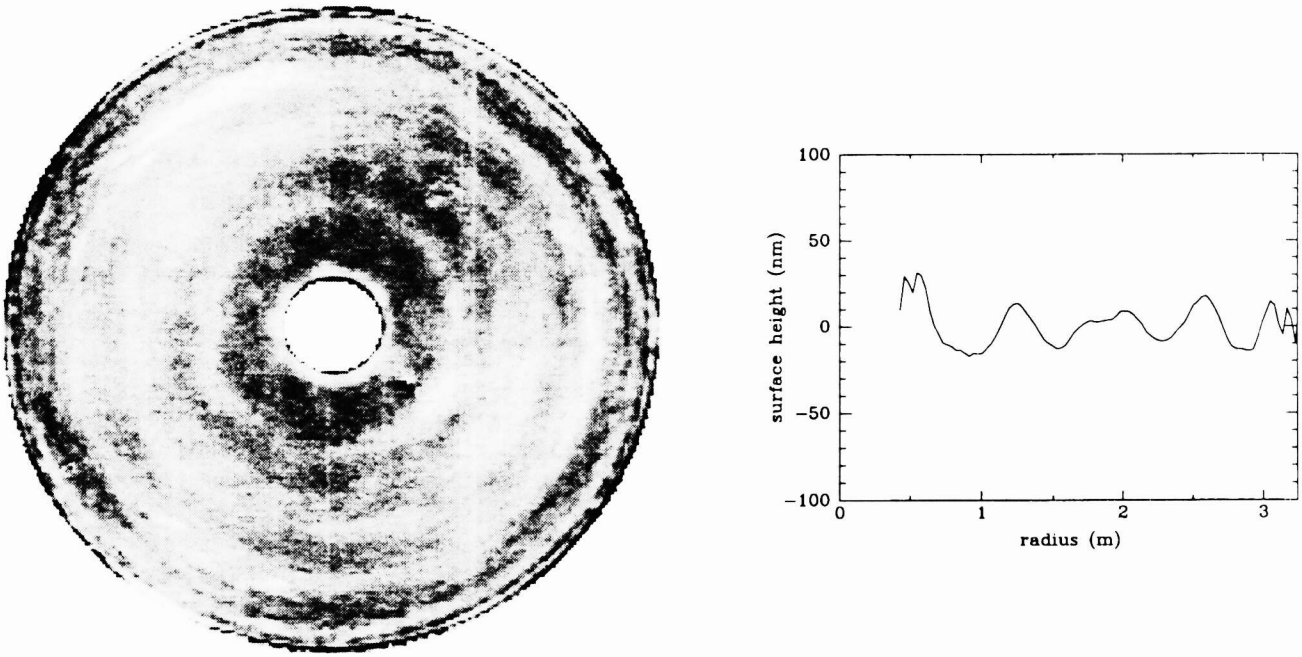

Figure 6. Gray-scale surface map and average radial profile at iteration 71, immediately before the first use of passive laps on the interior. The gray scale covers ±100 nm of surface, and the image covers the full 6.5 m diameter.

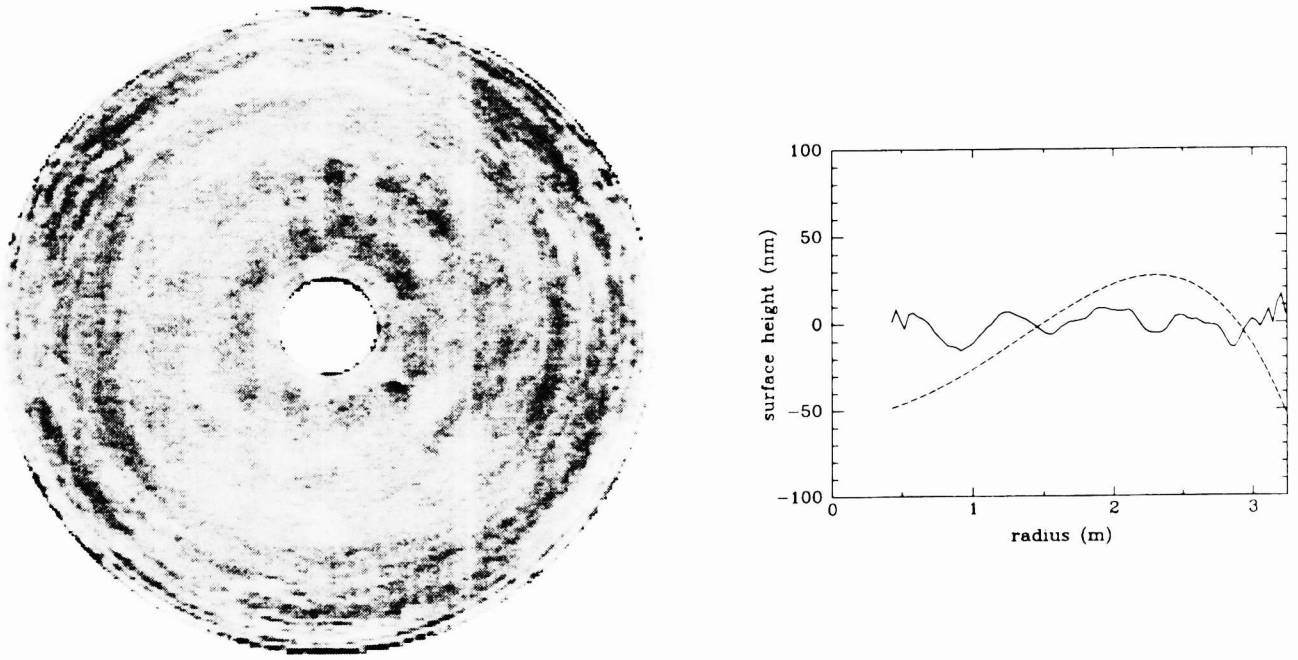

Figure 7. Gray-scale surface map and average radial profile of the finished Magellan mirror. The gray scale covers ±100 nm of surface, and the image covers the full 6.5 m diameter. This is an average of three standard measurements; the more complete averaging of measurement noise reduced the rms surface error from 17 nm (as shown in Figure 4) to 14 nm. The dashed curve shown with the average radial profile is the aspheric departure divided by 10,000.

It is not surprising that the limitations of stressed-lap polishing appear first at the outer edge of the mirror, which is the most challenging part for almost any mirror and polishing process but especially for a steep asphere. The lap can only extend partially over the edge, limiting the optician's freedom to concentrate removal on this outer zone. A force imbalance occurs when the lap is partially unsupported, causing pressure gradients that increase rapidly with lap position and include a high concentration on the outer few cm. An additional force imbalance occurs because the slope at the edge of this mirror is 11 degrees. Such a large tilt of the stressed lap, combined with a relatively high center of gravity due to the bending actuators, causes a significant pressure gradient. We compensate for all force imbalances with the three lifting actuators that control the net force and moment, but this system has finite accuracy and leaves residual pressure gradients that scale with the amount of compensation. Since we only compensate the net force and moments, as opposed to the full pressure distribution, the competing moments cause the plate to bend, and the resulting systematic shape error affects the mirror figure. Finally, the mirror's asphericity is greatest at the edge—curvatures in the radial and tangential direction differ by 4%—so the lap bending is also greatest. The lap's shape errors increase with the amount of bending and the resulting misfit and pressure gradients also affect the mirror figure.

The final set of five high zones apparent in Figure 6 have periods of about 0.6 m, or half the diameter of the stressed lap. This is the structure that lies in the gap between figuring and smoothing. Figuring is selective removal of glass based on something like Preston's formula for the local removal rate,

$$\frac{dz}{dt} = kpv, \tag{1}$$

where k is assumed constant, p is pressure and v is relative speed between lap and glass. We have four parameters that are controlled as a function of radius to give differential removal:

1. dwell time, controlled by the radial speed of the lap. This variable alone gives a spatial variation in removal equal to the spatial variation in dwell convolved with the lap's footprint, so the spatial resolution is roughly one lap diameter d.

2. speed, controlled by lap rotation. Rotation creates a linear variation of relative speed across the lap (in the radial direction), so the resolution is about $d/2$.
3. mean pressure, controlled by the three lifting actuators. The resolution is roughly d.
4. pressure gradient, also controlled by the lifting actuators. This creates a linear variation of pressure, so the resolution is roughly $d/2$.

The limiting resolution of the figuring process is therefore about half the lap diameter.

Smoothing results from the concentration of pressure on high regions whose spatial scale is less than the lap diameter. This process occurs naturally when the lap is stiff enough to bridge the low between adjacent high regions. A lap resting on two high regions sags like a beam on two supports. If the two high regions are separated by l, a reasonable model is a beam of length l with fixed ends. The lap's sag is

$$s = \left(\frac{p}{E}\right)\frac{l^4}{32t^3}, \tag{2}$$

where the pressure p is about 1.4 kPa, the Young's modulus $E = 70$ GPa for aluminum and the plate thickness $t = 50$ mm, giving

$$s = 5\left(\frac{l}{1\text{m}}\right)^4 \text{ microns.} \tag{3}$$

For figure errors with amplitudes less than s, the lap will sag to make contact at the low as well as the high regions and smoothing will be ineffective. For amplitudes greater than s, if the lap maintains an accurate shape it will be effective at removing the errors. The sag s is a strong function of separation l. For figure errors with a period of 0.6 m, the lap sags by about 600 nm, so smoothing is not efficient at achieving the desired accuracy. For a period of 0.2 m, the sag is only 8 nm and smoothing should achieve high accuracy.

The combination of a minimum resolution of about 0.6 m for figuring and a maximum resolution of about 0.2 m for strong smoothing leaves a gap that we fill with passive laps. The errors that we correct with passive laps are nearly axisymmetric and are treated as if perfectly symmetric. The azimuthal component of figure error is well controlled by the stressed lap through pressure variations and passive smoothing.

5. CONCLUSION

We have figured the first Magellan primary mirror to an accuracy of 14 nm rms surface error (excluding Seidel astigmatism and spherical aberration), with 80% of the light at 500 nm focussed within a 0.06″ diameter. The mirror will make a negligible contribution to image degradation in the best seeing. Most of the figuring was done with a 1.2 m stressed lap. This technique gave high accuracy at large and small scales but did not achieve the desired accuracy on scales around 0.6 m. Axisymmetric figuring with small passive tools filled this gap effectively. The Mirror Lab is now in the process of making another 6.5 m f/1.25 mirror for the second Magellan telescope, and two 8.4 m f/1.14 mirrors for the Large Binocular Telescope.

6. REFERENCES

1. M. Johns, "Magellan 6.5-m Telescopes Project: status report", in *Optical Telescopes of Today and Tomorrow: Following in the Direction of Tycho Brahe*, Arne Ardeberg, Editor, Proc. SPIE 2871, p. 49 (1997).
2. H. M. Martin, D. S. Anderson, J. R. P. Angel, R. H. Nagel, S. C. West, R. S. Young, "Progress in the stressed-lap polishing of a 1.8-m f/1 mirror", in *Advanced Technology Optical Telescopes IV*, Lawrence D. Barr, Editor, Proc. SPIE 1236, p. 682 (1990).

3. S. C. West, H. M. Martin, R. H. Nagel, R. S. Young, W. B. Davison, T. J. Trebisky, S. T. DeRigne, B. B. Hille, "Practical Design and Performance of the Stressed-Lap Polishing Tool", *Applied Optics* 33, p. 8094 (1994).

4. B. H. Olbert, J. R. P. Angel, J. M. Hill, S. F. Hinman, "Casting 6.5-meter mirrors for the MMT conversion and Magellan", in *Advanced Technology Optical Telescopes V*, Larry M. Stepp, Editor, Proc. SPIE 2199, p. 144 (1994).

5. H. M. Martin, J. H. Burge, D. A. Ketelsen, S. C. West, "Fabrication of the 6.5 m primary mirror for the Multiple Mirror Telescope Conversion", in *Optical Telescopes of Today and Tomorrow: Following in the Direction of Tycho Brahe*, Arne Ardeberg, Editor, Proc. SPIE 2871, p. 399 (1997).

6. H. M. Martin, R. G. Allen, J. R. P. Angel, J. H. Burge, W. B. Davison, S. T. DeRigne, L. R. Dettmann, D. A. Ketelsen, W. C. Kittrell, S. M. Miller, P. A. Strittmatter, S. C. West, "Fabrication and measured quality of the MMT primary mirror", in *Advanced Technology Optical/IR Telescopes VI*, Larry M. Stepp, Editor, Proc. SPIE 3352, p. 194 (1998).

7. D. Ketelsen, W. Davison, S. DeRigne, W. Kittrell, "A machine for complete fabrication of 8-m class mirrors", in *Advanced Technology Optical Telescopes V*, Larry M. Stepp, Editor, Proc. SPIE 2199, p. 651 (1994).

8. J. H. Burge, D. S. Anderson, D. A. Ketelsen, S. C. West, "Null test optics for the MMT and Magellan 6.5-m f/1.25 primary mirrors", in *Advanced Technology Optical Telescopes V*, Larry M. Stepp, Editor, Proc. SPIE 2199, p. 658 (1994).

9. P. M. Gray, J. M. Hill, W. B. Davison, S. P. Callahan, J. T. Williams, "Support of large borosilicate honeycomb mirrors", in *Advanced Technology Optical Telescopes V*, Larry M. Stepp, Editor, Proc. SPIE 2199, p. 691 (1994).

10. H. M. Martin, W. B. Davison, S. T. DeRigne, G. Parodi, T. J. Trebisky, S. C. West, "Active supports and force optimization for the MMT primary mirror", in *Advanced Technology Optical/IR Telescopes VI*, Larry M. Stepp, Editor, Proc. SPIE 3352, p. 412 (1998).